Spectrochimica Acta Part A: Molecular and Biomolecular Spectroscopy 136 (2015) 1358–1370

Contents lists available at ScienceDirect

Spectrochimica Acta Part A: Molecular and Biomolecular Spectroscopy

journal homepage: www.elsevier.com/locate/saa

# A detailed experimental and theoretical study of two novel substituted trifluoromethylchromones. The influence of the bulky bromine atom on the crystal packing

C.D. Alcívar León [a,1], G.A. Echeverría [b], O.E. Piro [b], S.E. Ulic [a,c,*], J.L. Jios [d,*]

[a] CEQUINOR (CONICET-UNLP), Facultad de Ciencias Exactas, Universidad Nacional de La Plata, 47 esq. 115, 1900 La Plata, Argentina
[b] Departamento de Física, Facultad de Ciencias Exactas, Universidad Nacional de La Plata e IFLP (CONICET, CCT-La Plata), C.C. 67, 1900 La Plata, Argentina
[c] Departamento de Ciencias Básicas, Universidad Nacional de Luján, Rutas 5 y 7, 6700 Luján, Buenos Aires, Argentina
[d] LASEISIC-PLAPIMU (UNLP-CIC), Departamento de Química, Facultad de Ciencias Exactas, Universidad Nacional de La Plata, 47 esq. 115, 1900 La Plata, Argentina

## HIGHLIGHTS

- Two novel substituted 2-trifluoromethylchromones were synthesized and analyzed.
- The crystal structure of both molecules was elucidated by X-ray diffraction.
- The brominated derivative shows a strong rotational disorder around the C—$CF_3$ bond.
- DFT calculations were applied to the conformational and spectroscopic analysis.

## GRAPHICAL ABSTRACT

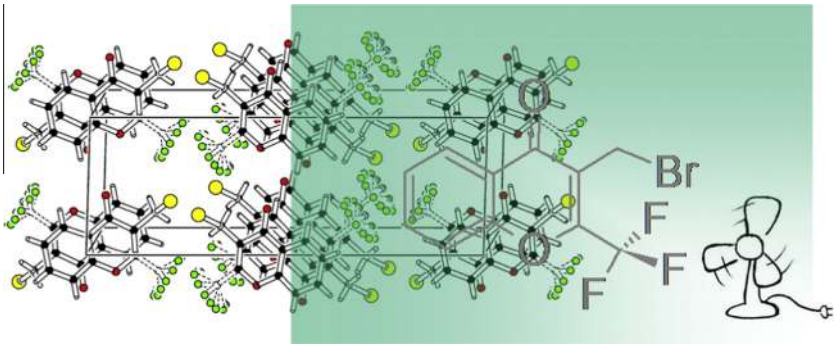


## ARTICLE INFO

*Article history:*
Received 7 May 2014
Received in revised form 11 September 2014
Accepted 11 October 2014
Available online 18 October 2014

*Keywords:*
2-Trifluoromethylchromones
Quantum chemical calculations
Spectroscopic properties
Single crystal X-ray diffraction

## ABSTRACT

The new 3-methyl-2-trifluoromethylchromone (**1**) and 3-bromomethyl-2-trifluoromethylchromone (**2**) compounds were synthesized and characterized by vibrational (IR, Raman), UV–Vis and NMR ($^{1}H$, $^{13}C$ and $^{19}F$) spectroscopy and MS spectrometry. The crystal structures of **1** and **2** were determined by X-ray diffraction methods. Both compounds crystallize in the monoclinic $P2_1/c$ space group with $Z = 4$ molecules per unit cell. The structures were solved from 1423 (**1**) and 1856 (**2**) reflections with $I > 2\sigma(I)$ and refined by full-matrix least-squares to agreement R1-values of 0.0403 (**1**) and 0.0554 (**2**). Because of π-bonding delocalization, the organic molecular skeletons are planar and the molecular bonding structures can be described by formally single, double and resonant bonds. In **2,** the —$CF_3$ group revealed a strong rotational disorder around the C—$CF_3$ bond, which could be explained in terms of four split positions with about uniform angular distribution. The vibrational, electronic and NMR, spectra were discussed and assigned with the assistance of DFT calculations.

© 2014 Elsevier B.V. All rights reserved.

* Corresponding authors at: CEQUINOR (CONICET-UNLP), Facultad de Ciencias Exactas, Universidad Nacional de La Plata, 47 esq. 115, 1900 La Plata, Argentina (S.E. Ulic).
*E-mail addresses:* sonia@quimica.unlp.edu.ar (S.E. Ulic), jljios@quimica.unlp.edu.ar (J.L. Jios).
[1] SENESCYT-Ecuador.

http://dx.doi.org/10.1016/j.saa.2014.10.022
1386-1425/© 2014 Elsevier B.V. All rights reserved.

## Introduction

Chromones are bicyclic organic compounds [1,2]. They are part of a large family of heterocycles structurally constituted by a benzene ring fused to a 4-pyrone group [3,4]. A variety of metabolites with a chromone structure have been found in nature and were widely studied [5,6]. They show to be nutraceutical [7] and exhibit diverse biological properties [8–12]. Among the ample variety of substituents that can be attached to the chromone backbone the trifluoromethyl group (—$CF_3$) is one of the most interesting to study due to its influence on the chromone biological behavior. In fact there are several studies on the potential pharmaceutical activity of structural analogs of chromone [9,13,14].

One of the most employed methods for the synthesis of chromones involves the reaction of ortho-hydroxyacetophenones with several acid anhydrides, followed by intra-molecular cyclization and subsequent dehydration [15–18]. The preparation of new 2-trifluoromethylchromones using the above method with trifluoroacetic ethyl ester has been reported by Sosnovskikh's group [19–22]. More recently, a new chemical pathway involving esterification and cyclization in one step using trifluoroacetic anhydride was developed in our laboratory [23]. This methodology was adopted for the synthesis of 3-methyl-2-trifluorometilchromone **(1)**. Subsequent bromination affords the synthesis of 3-bromomethyl-2-trifluoromethylchromone **(2)**. The structures of the title compounds are shown in Scheme 1.

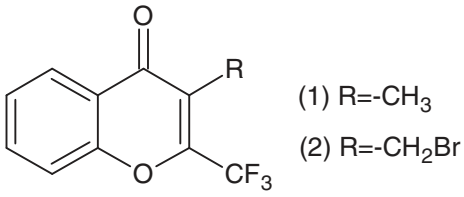


**Scheme 1.**

## Experimental section

The **1** and **2** compounds were characterized by solution NMR ($^1H$, $^{13}C$, $^{19}F$) and electronic (UV–Vis) spectroscopy, and mass spectrometry. The solid state vibration behavior was studied by infrared (IR) absorption and Raman dispersion spectroscopy. The crystal structure of **1** and **2** were determined by X-ray diffraction methods. The gas phase geometry optimization of both molecules was performed by quantum chemical calculations. Additional theoretical studies were selected for calculating vibration mode frequencies (IR, Raman), UV–Vis transitions and NMR chemical shifts ($^1H$, $^{13}C$, $^{19}F$).

### *Instrumentation*

#### *Infrared and Raman spectroscopy*

Infrared absorption spectra (KBr pellets) were recorded on a LUMEX InfraLUM FT-02 spectrometer with a resolution of 2 $cm^{-1}$ in the range from 4000 to 400 $cm^{-1}$. Raman dispersion spectra of the solid were measured from powdered samples in Pyrex standard capillaries (2.5-mm i.d.) with a Perkin–Elmer FT-Raman RFs 100/s spectrometer using as exciting light source the 1064 nm line from a Nd/YAG laser (spectral resolution of 4 $cm^{-1}$) in the 3500–100 $cm^{-1}$ spectral range.

#### *NMR spectra*

The $^1H$ (200.0 MHz), $^{19}F$ (188.7 MHz) and $^{13}C$ (50.3 MHz) NMR spectra of **(1)** were recorded on a Varian Mercury Plus 200 spectrometer. The samples were dissolved in $CDCl_3$ and the solution introduced within a 5 mm NMR tube. Chemical shifts ($\delta$) are given in ppm and referenced to TMS ($\delta$ = 0 ppm). For the $^{19}F$ NMR spectrum a 0.05% TFA in $CDCl_3$ solution was used as external reference ($\delta$ = −71.0 ppm). Coupling constants ($J$) are reported in Hz, being the singlet indicated as *s*, doublet as *d*, double doublet as *dd*, double double doublet as *ddd*, triplet as t, quartet as q and broad doublet as br d (see Synthesis and characterization section). For NMR data, the standard numbering scheme of the benzopyrane skeleton (with the bridged oxygen atom carrying the number 1) was adopted to facilitate the comparison with data reported in the literature.

#### *UV–visible spectroscopy*

The spectra of **1** and **2** in methanol were recorded using a quartz cell (10 mm optical path length) on a ChromTech CT-5700 UV/Vis spectrophotometer at 2.0 nm spectral bandwidth. Measurements were carried out in the spectral region from 190 to 700 nm.

#### *Mass spectrometry*

The MS determinations were performed by injection of methanol solutions (~1 μl) in a HP 5890 Chromatograph coupled to a HP 5972 A mass selective detector. An HP5-MS capillary column (30 m × 0.25 mm × 5 μm) has been used with $H_2$ as the carrier gas (0.6 ml/min). The temperature set points were: 200 °C in the split injector, 300 °C in the interface, 185 °C in the ion source and the oven ramp started at 80 °C and ended at 200 °C with a heating rate of 10 °C/min. The electron energy was 70 eV with a mass range of 50–350 amu and a pressure in the mass spectrometer lower than $10^{-5}$ Torr. The mass spectra of **1** and **2** are shown in Figs. S1 and S2 of Supporting Information.

#### *X-ray diffraction data*

The measurements were performed on an Oxford Xcalibur Gemini, Eos CCD diffractometer with graphite-monochromated Cu Kα ($\lambda$ = 1.54178 Å) radiation. X-ray diffraction intensities were collected (ω scans with ϑ and κ-offsets) at 120(2) K in compound **1** and 296(2) K in compound **2**, integrated and scaled with CrysAlisPro [24] suite of programs. The unit cell parameters were obtained by least-squares refinement (based on the angular setting for all collected reflections with intensities larger than seven times the standard deviations of measurement errors) using CrysAlisPro. Data were corrected empirically for absorption employing the multi-scan method implemented in CrysAlisPro. The structures were solved by direct methods with SHELXS-97 [25] and the corresponding molecular models developed by alternated cycles of Fourier methods and full-matrix least-squares refinement on $F^2$ with SHELXL-97 [26]. In **2** the —$CF_3$ group showed severe rotational disorder around the C—$CF_3$ bond which could be successfully modeled in terms of four split positions with approximate uniform angular distribution. The four C—$CF_3$ replicas were refined (with isotropic displacement parameters) by restraining all the C—F bond lengths and F···F distances to be respectively equal to one another while restraining the occupancies such to add up to one. For both compounds, a Fourier difference map phased on the heavier atoms showed all the H-atoms. In **1** these were refined at their found position with isotropic displacement parameters and in **2** they were positioned stereo-chemically and refined with the riding model. Crystal data and structure refinement results are summarized in Table S1 of Supporting Information. Crystallographic structural data have been deposited with the Cambridge Crystallographic Data Centre (CCDC). Any request to the CCDC for this material should quote the full literature citation and the reference number CCDC 976319 (for **1**) and CCDC 976320 (for **2**).

*Computational methods*

Quantum chemical calculations were performed in the gas phase with the program package Gaussian 03 [27]. Scans of the potential energy surface, geometry optimizations and vibration mode frequency calculations were carried out with the density functional theory (B3LYP) method employing the 6-311++G(d,p) basis set. In all cases, the calculated vibrational properties corresponded to potential energy minima with no imaginary values for the frequencies. Electronic transitions were calculated with TD-DFT [28,29] taking into account implicitly the solvent effect (methanol). The $^{1}H$ and $^{13}C$ chemical shifts were calculated with the B3LYP/6-311+g(2d,p) optimized geometries by the GIAO method (Gauge Including Atomic Orbital) [30] using the corresponding TMS shielding, calculated at the same level of theory.

## Results and discussion

*Synthesis and characterization*

The synthetic route is depicted in Scheme 2 (Supporting Information).

*3-Methyl-2-trifluoromethylchromone (**1**)*

Following our reported procedure [23], 2-hydroxypropiophenone (8.7 g, 57.9 mmol), trifluoroacetic anhydride (12.8 g, 60.8 mmol) and pyridine (4,8 ml), were heated with stirring at 120 °C for 6 h. The reaction mixture was treated with 1 M hydrochloric acid (3 times, 10 ml) and water (2 times, 10 ml), then the unreacted 2-hydroxypropiophenone was removed by washing several times with 10 mL of 1 M NaOH (controlling its disappearance by TLC). The organic phase was dried with $Na_2SO_4$ and the solvent removed in a rotary evaporator to give a white solid. Recrystallization from hot hexane produced a crystalline solid (m.p. 99–100 °C). $^{1}H$ NMR, $\delta$ = 8.19 (ddd, 1H, H-5, $^{3}J$ = 8 Hz; $^{4}J$ = 2 Hz; $^{5}J$ = 0.5 Hz), 7.72 (ddd, 1H, H-7, $^{3}J$ = 9 Hz; $^{3}J$ = 7 Hz; $^{4}J$ = 2 Hz), 7.48 (br d, 1H, H-8, $J$ = ~8 Hz), 7.44 (ddd, 1H, H-6, $^{3}J$ = 8 Hz; $^{3}J$ = 7 Hz; $^{4}J$ = 1 Hz), 2.23 ppm (q, 3H, CH3, $^{5}J_F$ = 2 Hz). $^{13}C$ NMR: $\delta$ = 177.9 (C-4), 155.1 (C-8a), 148.2 (q, C-2, $^{2}J_{C,F}$ = 37 Hz), 134.6 (C-7), 126.1 (C-5), 125.9 (C-6), 122.4 (C-4a), 120.9 (q, C-3, $^{3}J_{C,F}$ = 1 Hz), 120.0 (q, $CF_3$, $^{1}J_{C,F}$ = 276 Hz), 118.2 (C-8), 8.7 ppm (t, $CH_3$, $^{4}J_{C,F}$ = 3 Hz). $^{19}F$ NMR: $\delta$ = −65.83 ppm (q, $^{3}J_F$ = 2.5 Hz). MS: $m/z$ (%) = 228 ($[M]^+$, 75), 209 ($[M–F]^+$, 5.8), 199 ($[C_{10}H_6F_3O]^+$, 8.2), 120 ($[C_7H_4O_2]^+$, 13.5), 92 ($[C_6H_4O]^+$, 26). UV–Vis (methanol): $\lambda_{max}$ 204, 224, 243 and 308 nm.

*3-Bromomethyl-2-trifluoromethylchromone (**2**)*

3-Methyl-2-trifluoromethyl chromone (**1**) (1.72 g, 7.54 mmol) was dissolved in carbon tetrachloride (50 ml). A saturated solution of bromine in water (160 ml) was added to the organic solution and the mixture kept at room temperature in presence of visible light for 12 h under stirring. The conversion of the starting reagent **1** was monitored by TLC. Then the organic phase was separated, dried (with $Na_2SO_4$) and the solvent removed with a rotary evaporator producing **2** as a white solid in quantitative yield. Recrystallization from hexane resulted in a white crystalline solid (m.p. 137–138 °C). $^{1}H$ NMR, $\delta$ = 8.23 (dd, 1H, H-5, $^{3}J$ = 8 Hz; $^{4}J$ = 1.5 Hz), 7.79 (ddd, 1H, H-7, $^{3}J$ = 9 Hz; $^{3}J$ = 7 Hz; $^{4}J$ = 2 Hz), 7.54 (br d, 1H, H-8, $^{3}J$ = 9 Hz), 7.52 (ddd, 1H, H-6, $^{3}J$ = 8 Hz; $^{3}J$ = 7 Hz; $^{4}J$ = 1 Hz), 4.56 ppm (s, 2H, $CH_2Br$). $^{13}C$ NMR: $\delta$ = 175.4 (C-4), 154.9 (C-8a), 149.9 (q, C-2, $^{2}J_F$ = 38 Hz), 135.4 (C-7), 122.7 (C-5), 126.4 (C-6), 122.7 (C-4a), 121.4 (q, C-3, $^{3}J_F$ = 1 Hz), 119.4 (q, $CF_3$, $^{1}J_F$ = 277 Hz), 118.4 (C-8), 18.8 ppm (q, $CH_2Br$, $^{4}J_F$ = 3 Hz). MS: $m/z$ (%) = 306 ($[M]^+$, 21), 227 ($[M–Br]^+$, 100), 199 ($[C_{10}H_6F_3O]^+$, 8.2), 120 ($[C_7H_4O_2]^+$, 13.5), 92 ($[C_6H_4O]^+$, 26). UV–Vis (methanol): $\lambda_{max}$ 206, 228, 247 and 302 nm.

*Crystallographic structural results*

Figs. 1 and 2 are ORTEP drawings of the closely related **1** and **2** molecules. Their bond distances and angles are showed in Table 1. Because of extended π-bonding, the organic molecular skeletons are planar [*rms* deviations of atoms from the best least-squares plane of 0.0319 Å (**1**) and 0.0353 Å (**2**)].

The observed interatomic distances and angles are consistent with the description of the molecular structure in terms of formally single, double and resonant bonds. Particularly, in **1** the C—C distances of the phenyl ring are in the 1.379(3)–1.407(3) Å range, corresponding to a resonant-bond structure. Within the heterocycle, observed C—(C=O) distances of 1.473(3) and 1.471(2) Å agree with the single bond character for these links, and the short C6—C7 bond distance of 1.338(3) Å with its double bond character. Single bond C—O distances are 1.360(2) and 1.376(2) Å and d(C =O) = 1.224(2) Å. Trifluoromethyl C—F bond distances are in the range from 1.326(2) to 1.333(2) Å. The crystal packing drawing of **1** is shown in Fig. S3.

As expected, **2** shows similar to **1** bond distances and angles of the common organic framework, being the C—Br bond distance equal to 1.955(5) Å. Compared with **1**, the most noticeable difference in the crystal structure of **2** is the behavior of the —$CF_3$ group. As described in the experimental section, the —$CF_3$ group of **2** showed rotational disorder around the C—$CF_3$ bond which was

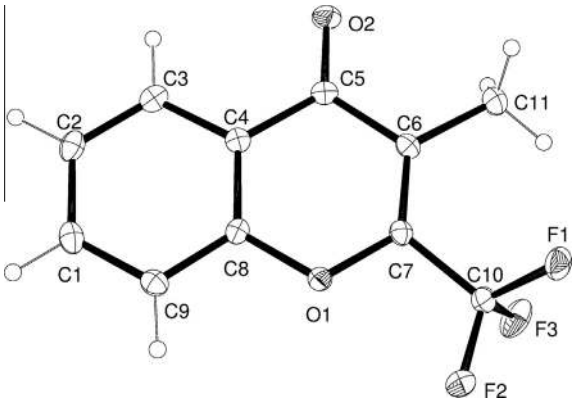


**Fig. 1.** View of 3-methyl-2-trifluoromethylchromone molecule (**1**) showing the labeling of the non-H atoms and their displacement ellipsoids at the 30% probability level.

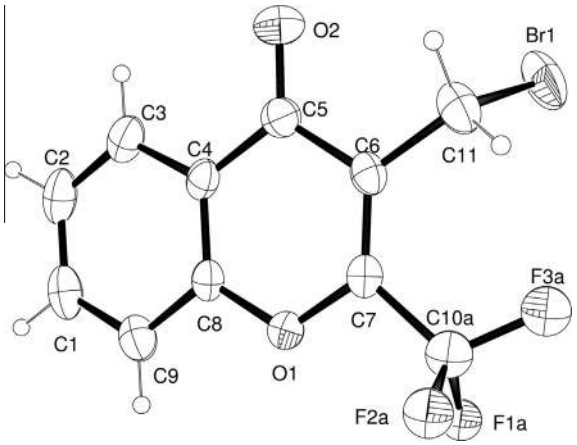


**Fig. 2.** View of 3-bromomethyl-2-trifluoromethylchromone molecule (**2**). For simplicity, only one out of the four rotationally split positions observed for the —$CF_3$ group is shown.

**Table 1**
Experimental and calculated bond lengths (Å), bond angles (°), and selected torsion angles (°)[a,b] of **1** and **2**.

| Param. | 1 | | 2 | | Param. | 1 | | 2 | |
|---|---|---|---|---|---|---|---|---|---|
| | Exp. | Calc. | Exp. | Calc. | | Exp. | Calc. | Exp. | Calc. |
| *r*(C1—C2) | 1.395(3) | 1.405 | 1.378(8) | 1.405 | ∠(O2—C5—C6) | 122.34(17) | 121.7 | 121.3(4) | 121.6 |
| *r*(C1—C9) | 1.380(3) | 1.385 | 1.380(7) | 1.386 | ∠(C1—C2—C3) | 120.10(18) | 120.0 | 120.7(5) | 120.1 |
| *r*(C2—C3) | 1.379(3) | 1.383 | 1.365(8) | 1.383 | ∠(C1—C9—C8) | 117.80(18) | 118.5 | 117.4(5) | 118.4 |
| *r*(C3—C4) | 1.407(3) | 1.405 | 1.400(6) | 1.405 | ∠(C2—C1—C9) | 121.28(18) | 120.7 | 121.2(5) | 120.8 |
| *r*(C4—C5) | 1.473(3) | 1.474 | 1.462(6) | 1.472 | ∠(C2—C3—C4) | 119.89(19) | 120.4 | 120.0(5) | 120.3 |
| *r*(C4—C8) | 1.387(3) | 1.397 | 1.380(6) | 1.395 | ∠(C3—C4—C5) | 121.22(17) | 121.6 | 121.9(4) | 121.7 |
| *r*(C5—O2) | 1.224(2) | 1.224 | 1.219(5) | 1.222 | ∠(C3—C4—C8) | 118.34(17) | 118.4 | 118.2(4) | 118.5 |
| *r*(C5—C6) | 1.471(2) | 1.480 | 1.473(6) | 1.490 | ∠(C4—C5—C6) | 115.08(16) | 115.4 | 115.2(3) | 115.6 |
| *r*(C6—C7) | 1.338(3) | 1.351 | 1.336(6) | 1.354 | ∠(C4—C8—C9) | 122.59(17) | 121.9 | 122.5(4) | 122.1 |
| *r*(C6—C11) | 1.503(3) | 1.501 | 1.496(6) | 1.492 | ∠(C5—C4—C8) | 120.41(16) | 119.9 | 119.9(4) | 120.0 |
| *r*(C7—O1) | 1.360(2) | 1.353 | 1.353(5) | 1.350 | ∠(C5—C6—C7) | 118.63(16) | 118.5 | 119.1(4) | 118.4 |
| *r*(C7—C10) | 1.520(2) | 1.524 | 1.519(6) | 1.523 | ∠(C5—C6—C11) | 116.37(17) | 116.5 | 115.9(4) | 115.3 |
| *r*(C8—O1) | 1.376(2) | 1.368 | 1.370(5) | 1.370 | ∠(C6—C7—C10) | 124.63(16) | 124.3 | 128.2(4) | 128.7 |
| *r*(C8—C9) | 1.390(3) | 1.397 | 1.392(6) | 1.395 | ∠(C6—C11—Br) | – | – | 110.8(3) | 111.4 |
| *r*(C10—F1) | 1.335(2) | 1.352 | 1.370(9) | 1.430 | ∠(C7—O1—C8) | 118.06(14) | 119.5 | 118.7(3) | 120.3 |
| *r*(C10—F2) | 1.326(2) | 1.338 | 1.311(9) | 1.349 | ∠(C7—C6—C11) | 124.98(17) | 125.1 | 125.0(4) | 126.3 |
| *r*(C10—F3) | 1.333(2) | 1.352 | 1.347(9) | 1.346 | | | | | |
| *r*(C11—Br) | – | – | 1.955(5) | 1.997 | *Φ*(O1—C7—C6—C11) | −177.6 | −180.0 | 178.0 | −179.5 |
| | | | | | *Φ*(O1—C7—C10—F2) | −10.0 | −0.5 | −163.8 | −179.1 |
| ∠(O1—C7—C6) | 126.26(16) | 125.4 | 125.0(4) | 124.7 | *Φ*(O1—C8—C9—C1) | −179.5 | −180.0 | −179.6 | 179.8 |
| ∠(O1—C7—C10) | 109.08(15) | 110.3 | 106.8(3) | 106.6 | *Φ*(O1—C7—C6—C5) | 0.7 | 0.1 | −0.1 | 0.7 |
| ∠(O1—C8—C4) | 121.51(16) | 121.3 | 121.9(4) | 121.1 | *Φ*(O2—C5—C4—C3) | 0.8 | −0.1 | 4.1 | 2.0 |
| ∠(O1—C8—C9) | 115.90(16) | 116.7 | 115.6(4) | 116.8 | *Φ*(O2—C5—C4—C8) | 178.7 | 179.9 | −176.4 | −177.8 |
| ∠(F1—C10—F3) | 106.49(15) | 106.9 | 104.0(8) | 107.7 | *Φ*(O2—C5—C6—C11) | −1.4 | 0.1 | −1.6 | −2.5 |
| ∠(F1—C10—C7) | 112.12(16) | 111.3 | 110.7(6) | 110.4 | *Φ*(C2—C3—C4—C5) | 177.8 | −180.0 | −180.0 | −179.9 |
| ∠(F2—C10—F1) | 106.89(15) | 107.5 | 107.7(8) | 107.5 | *Φ*(C5—C6—C11—Br) | – | – | −88.0 | 90.0 |
| ∠(F2—C10—F3) | 107.33(17) | 107.5 | 107.5(8) | 107.5 | *Φ*(C7—O1—C8—C9) | 177.6 | 180.0 | 178.1 | 178.7 |
| ∠(F2—C10—C7) | 112.32(15) | 112.1 | 112.5(7) | 110.2 | *Φ*(C7—C6—C11—Br) | – | – | 93.9 | −89.9 |
| ∠(F3—C10—C7) | 111.35(15) | 111.3 | 113.8(6) | 113.4 | *Φ*(C10—C7—C6—C11) | 0.0 | 0.0 | −2.9 | 0.2 |
| ∠(O2—C5—C4) | 122.56(17) | 122.9 | 123.5(4) | 122.9 | *Φ*(C10—C7—O1—C8) | −176.7 | −180.0 | −176.2 | −178.5 |

[a] Atom numbering scheme taken from Figs. 1 and 2.
[b] Experimental data from X-ray diffraction and computed parameters at the B3LYP/6-311++g(d,p) level of theory.

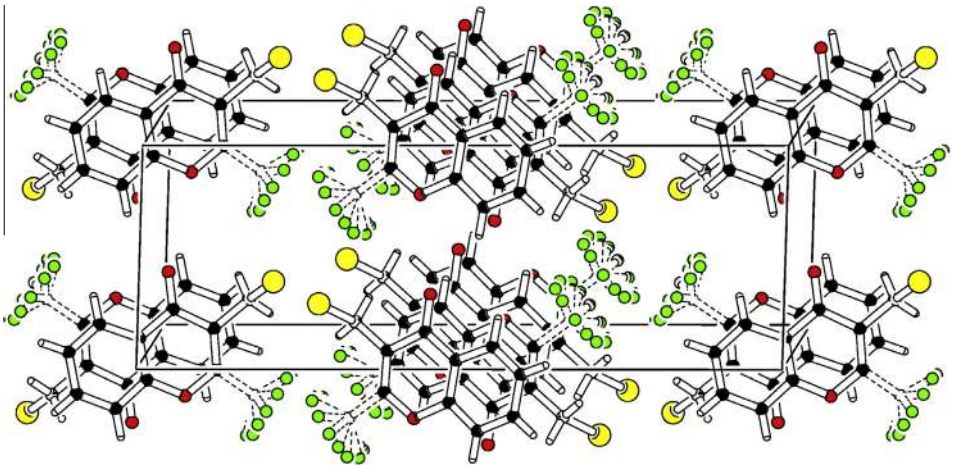

**Fig. 3.** Crystal packing of 3-bromomethyl-2-trifluoromethylchromone projected down the crystal *c*-axis. The *b*-axis is horizontal. Fluorine and bromine atoms are represented as green and yellow disks. The figure shows the four split angular positions observed for the —$CF_3$ group. (For interpretation of the references to color in this figure legend, the reader is referred to the web version of this article.)

interpreted in terms of four split positions with nearly uniform angular distribution and occupancies of 0.26(1), 0.18(1), 0.21(1), and 0.36(1).

A similar effect was found for a trifluoromethyl substituted hydrazone molecule [31]. This is probably due to the fact that neighboring bulky bromine ions left voids in the lattice large enough to afford the observed angular spread of relatively unhindered —$CF_3$ group, as can be appreciated in the PLATON [32,33] crystal packing drawing of **2** (Fig. 3). As expected, the small size of the —$CH_3$ group in the non-brominated compound **1** allows a more efficient packing. Therefore, it can be assumed that the disorder observed in **2** is produced by the steric effect of the bromine atom. In fact, MO calculations of **2** in the gas phase described below shows rotational energy minima for —$CF_3$ with barriers of less than about 0.35 kcal mol$^{-1}$, low enough to affords at room temperature ($kT_{295K}$ = 0.586 kcal mol$^{-1}$) the thermal occupation of all rotational conformers. The question of whether there is actual rotational movement of —$CF_3$ in the solid could be answered through motional narrowing [34] studies of the $^{19}$F NMR spectrum. This however lies outside the scope of this work and therefore it will not be pursue here any further.

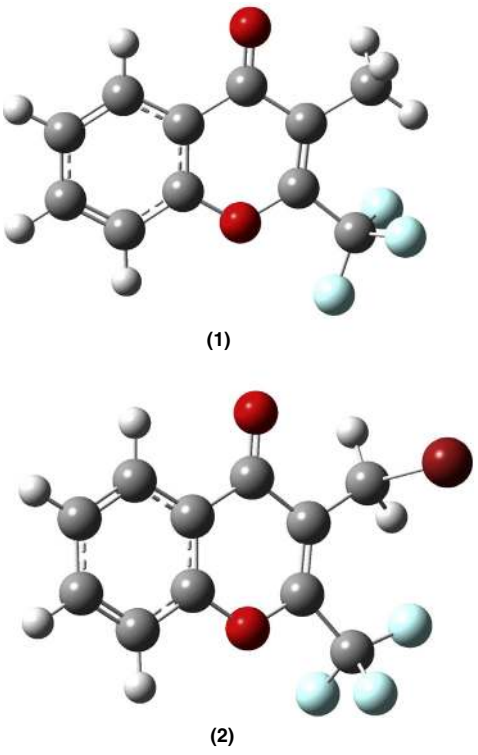


**Fig. 4.** Optimized structures (B3LYP/6-311++g(d,p)) of 3-methyl-2-trifluoromethylchromone (**1**) and 3-bromomethyl-2-trifluoromethylchromone (**2**).

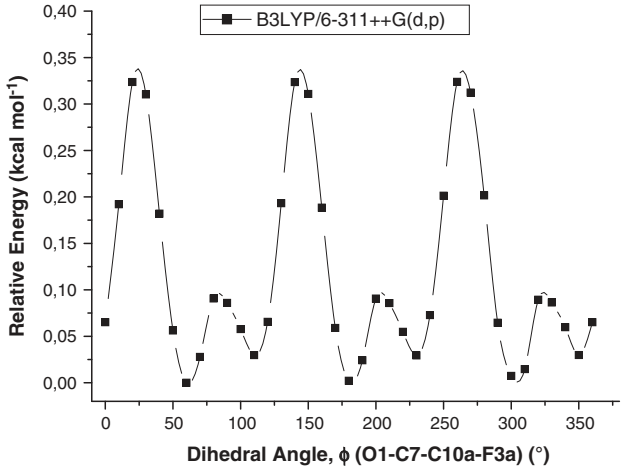


**Fig. 5a.** Potential energy curve for the internal rotation around the C7—C10 bond in **2** calculated at the B3LYP/6-311++G(d,p) level of theory.

## *Structural properties*

Potential energy curves (B3LYP/6-311++g(d,p)) for internal rotations around the —$CF_3$ and —$CH_3$ or —$CH_2Br$ groups for **1** and **2**, respectively, were carried out to assess the minimum-energy molecular geometry adopted by both compounds in gas phase. Fig. 4 shows the optimized geometry of the title compounds. The molecules are characterized primarily by a planar conformation.

For **1**, the —$CF_3$ group has one fluorine atom in the plane of the molecule (*anti* respect to the C=C bond) and one hydrogen atom of the —$CH_3$ group results *syn* to the same double bond (see Table 1). Furthermore, for **2** one fluorine atom is *syn* respect to the C=C bond. The —$CH_2Br$ group presents the bromine atom in *gauche*

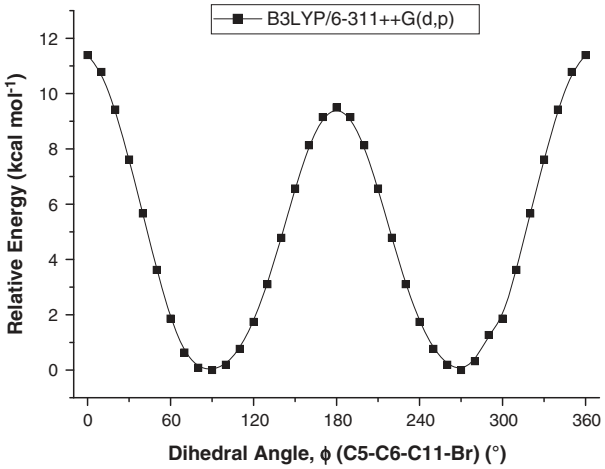


**Fig. 5b.** Potential energy curve for the internal rotation around the C6—C11 bond in **2** calculated at the B3LYP/6-311++G(d,p) level of theory.

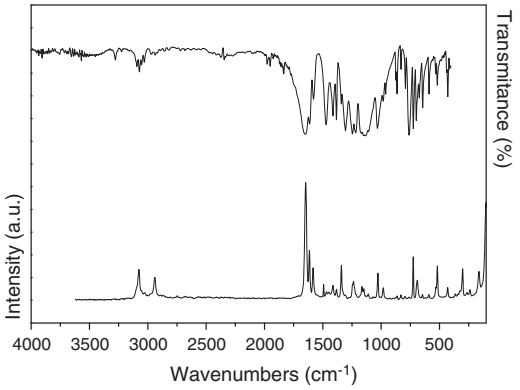


**Fig. 6.** Infrared spectrum of the solid (upper trace, KBr pellets) and Raman spectrum (lower trace) of 3-methyl-2-trifluoromethylchromone (**1**) at room temperature.

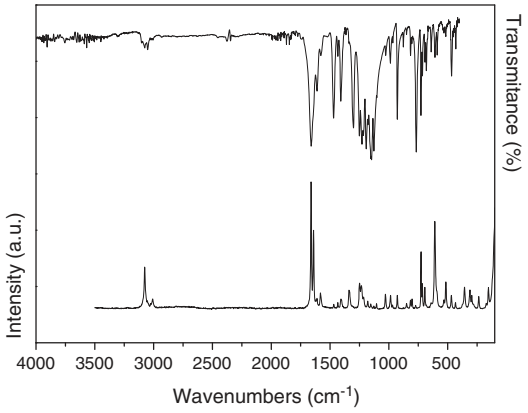


**Fig. 7.** Infrared spectrum of the solid (upper trace, KBr pellets) and Raman spectrum (lower trace) of 3-bromomethyl-2-trifluoromethylchromone (**2**).

orientation respect to the double bond and one hydrogen atom slightly deviated from the molecular plane (see Table 1). The potential energy curves of **2** for the dihedral angles O1C7C10F3 and C5C6C11Br are shown in Figs. 5a and 5b, respectively. As noted in Fig. 5a, the scan around the —$CF_3$ group indicates the presence of

**Table 2**
Experimental and calculated frequencies ($cm^{-1}$) and tentative assignment of fundamental vibration modes in 3-methyl-2-trifluoromethyl chromone (**1**).

| Mode | Experimental | | Calculated[b] | | Assignment[c] |
|---|---|---|---|---|---|
| | IR[a] | Raman | Frequency | Intensity | |
| $\nu_1$ | – | 3076(27) | 3204 | 6 | ν(C2—H); ν(C3—H); ν(C9—H); ν(C1—H) |
| $\nu_2$ | – | – | 3200 | 3 | ν(C3—H); ν(C9—H) |
| $\nu_3$ | 3094(vw) | 3056(10) | 3188 | 6 | ν(C2—H) |
| $\nu_4$ | 3072(vw) | 3028(7) | 3175 | 3 | ν(C2—H); ν(C1—H) |
| $\nu_5$ | 3054(vw) | 3005(5) | 3163 | 7 | $\nu_{as}(CH_3)$ |
| $\nu_6$ | – | 2981(6) | 3095 | 5 | $\nu_{as}(CH_3)$ |
| $\nu_7$ | 3030(vw) | 2940(20) | 3049 | 7 | $\nu_s(CH_3)$ |
| $\nu_8$ | 1651(vs) | 1648(100) | 1707 | 316 | ν(C=O) |
| $\nu_9$ | 1614(s) | 1615(43) | 1674 | 35 | ν(C6—C7); ν(C4—C8) |
| $\nu_{10}$ | 1580(s) | 1584(28) | 1649 | 65 | ν(C3—C2); ν(C8—C9) |
| $\nu_{11}$ | – | – | 1613 | 8 | ν(C2—C1); ν(C4—C8) |
| $\nu_{12}$ | – | – | 1503 | 5 | δ(C3—H); δ(C2—H); δ(C9—H) |
| $\nu_{13}$ | – | – | 1494 | 123 | $\delta_{as}(CH_3)$ |
| $\nu_{14}$ | – | 1493(15) | 1489 | <1 | δ(C3—H); δ(C2—H); δ(C1—H) |
| $\nu_{15}$ | 1472(s) | 1470(8) | 1473 | 11 | $\delta_{as}(CH_3)$ |
| $\nu_{16}$ | 1414(m) | 1414(13) | 1427 | 5 | $\delta_s(CH_3)$ |
| $\nu_{17}$ | 1383(s) | 1384(10) | 1414 | 64 | ν(C7—C10); ν(C5—C6); δ(C2—H); δ(C1—H) |
| $\nu_{18}$ | – | 1342(31) | 1364 | 1 | ν(C3—C4); ν(C1—C9) |
| $\nu_{19}$ | 1306(vs) | 1307(5) | 1315 | 130 | δ(C3—H); δ(C2—H); δ(C1—H); δ(C9—H) |
| $\nu_{20}$ | 1247(vs) | 1245(15) | 1249 | 248 | δ(C1—C9—H); δ(C4—C3—H) |
| $\nu_{21}$ | – | 1238(17) | 1244 | 67 | ν(C8—O); δ(C3—C2—H); δ(C9—C1—H) |
| $\nu_{22}$ | 1218(vs) | 1215(6) | 1224 | 103 | δ(C6—C11—H); δ(C3—C2—H) |
| $\nu_{23}$ | 1171(m) | – | 1183 | 31 | δ(C2—C1—H); δ(C3—C2—H) |
| $\nu_{24}$ | 1151(m) | 1165(12) | 1171 | 15 | δ(C8—C9—H); δ(C2—C1—H) |
| $\nu_{25}$ | 1134(vs) | 1149(11) | 1160 | 227 | $\nu_{as}(CF_3)$ |
| $\nu_{26}$ | – | – | 1131 | 37 | δ(C2—C3—H); δ(C1—C2—H); δ(C8—C9—H) |
| $\nu_{27}$ | 1107(m) | 1109(7) | 1121 | 275 | $\nu_{as}(CF_3)$ |
| $\nu_{28}$ | – | – | 1054 | 6 | δ(C6—C11—H) |
| $\nu_{29}$ | – | – | 1052 | 78 | wagg. $CH_3$ |
| $\nu_{30}$ | – | 1029(24) | 1047 | 29 | $\nu_s(CF_3)$; ν(C2—C1) |
| $\nu_{31}$ | – | – | 1009 | <1 | γ(C3—H); γ(C2—H); γ(C1—H) |
| $\nu_{32}$ | 984(m) | 982(12) | 992 | 6 | δ(O2—C5—C4); δ(C2—C3—C4) |
| $\nu_{33}$ | 962(m) | – | 985 | 2 | γ(C3—H); γ(C1—H); γ(C9—H) |
| $\nu_{34}$ | 875(vw) | – | 884 | <1 | γ(C3—H); γ(C2—H); γ(C9—H) |
| $\nu_{35}$ | 864(m) | 864(4) | 873 | 6 | δ(C2—C3—C1); δ(C7—O—C8) |
| $\nu_{36}$ | 830(vw) | 831(6) | 834 | 2 | δ(C5—C6—C11); δ(C9—C8—O) |
| $\nu_{37}$ | 792(m) | 795(4) | 801 | 8 | γ(C2—H); γ(C1—H); γ(C9—H) in phase; γ(C5—O) |
| $\nu_{38}$ | 762(s) | 761(3) | 775 | 62 | γ(C3—H); γ(C2—H); γ(C1—H) in phase |
| $\nu_{39}$ | 725(s) | 725(38) | 721 | 19 | $\delta_s(CF_3)$ |
| $\nu_{40}$ | 699(m) | – | 710 | 9 | γ(C4—C8—C9); γ(C5—C6—C7) |
| $\nu_{41}$ | 673(m) | 690(18) | 697 | 6 | δ(C2—C3—C4); δ(C8—C9—C1) |
| $\nu_{42}$ | – | 673[sh](5) | 676 | 2 | δ(C6—C1—C9) |
| $\nu_{43}$ | 644(m) | 647(6) | 652 | 8 | δ(O—C8—C9); δ(C7—C6—C11) |
| $\nu_{44}$ | 590(w) | 592(6) | 600 | 3 | δ(C8—C9—C1); δ(C2—C3—C4); $\delta_s(CF_3)$ |
| $\nu_{45}$ | 534(vw) | – | 539 | 3 | γ(C4—C8—C9); γ(C2—C3—C1) |
| $\nu_{46}$ | – | 532(12) | 530 | <1 | $\delta_{as}(CF_3)$ |
| $\nu_{47}$ | 519(w) | 519(30) | 521 | 2 | δ(C5—C4—C8) |
| $\nu_{48}$ | – | – | 514 | <1 | $\delta_{as}(CF_3)$ |
| $\nu_{49}$ | 438(vw) | – | 448 | 2 | γ(C2—C3—C4); γ(C8—O9—C1) |
| $\nu_{50}$ | 429(w) | 431(12) | 433 | 5 | δ(C5—C6—C7) |
| $\nu_{51}$ | – | 365(7) | 357 | 5 | δ(C5—C6—C11); δ(C7—C10—F) |
| $\nu_{52}$ | – | 342(7) | 344 | <1 | γ(C5—C6—C5) |
| $\nu_{53}$ | – | 325(9) | 321 | 2 | δ(C7—C6—C11) |
| $\nu_{54}$ | – | – | 304 | <1 | γ(C8—O—C7) |
| $\nu_{55}$ | – | 302(28) | 302 | 5 | δ(C3—C4—C5); δ(O—C7—C10) |
| $\nu_{56}$ | – | 263(7) | 253 | 4 | δ(C7—C6—C11) |
| $\nu_{57}$ | – | 239(10) | 232 | <1 | δ(C7—C10—F) |
| $\nu_{58}$ | – | 190(7) | 155 | <1 | δ(O—C7—C10) |
| $\nu_{59}$ | – | 162(25) | 149 | <1 | $\tau(CH_3—C6—C5)$; $\pi_{ip}(CF_3)$ |
| $\nu_{60}$ | – | – | 110 | <1 | $\tau(CH_3—C6—C5)$ |
| $\nu_{61}$ | – | – | 87 | 5 | τ(O—C5—C6—C11) |
| $\nu_{62}$ | – | – | 70 | <1 | τ(C3—C4—C5—C6) |
| $\nu_{63}$ | – | – | 22 | <1 | $\tau(CF_3—C7—O)$; $\tau(CH_3—C6—C5)$ |

[a] vs, very strong; s, strong; m, medium; w, weak; vw, very weak; sh, shoulder.
[b] 6-311++g(d,p) calculated IR frequencies ($cm^{-1}$) and intensities (km $mol^{-1}$) in parentheses.
[c] ν, δ, γ and τ represent stretching, in-plane deformation, out-of-plane deformation and torsion modes.

six nearly equivalent energy minima, with a very low energy barrier, showing multiple conformation possibilities. However, in the resolved crystal structure, the —$CF_3$ group is disordered over four position consistent with the presence of four conformations as discussed above. This discrepancy can be attributed to the influence of crystal packing interactions not accounted in the gas phase calculations.

Furthermore, the scan around the —$CH_2Br$ group (Fig. 5b) presents two equivalent energy minima at 90° and 270°, with the bromine atom *gauche* with respect to the molecular plane.

**Table 3**
Experimental and calculated frequencies ($cm^{-1}$) and tentative assignment of fundamental vibration modes in 3-bromomethyl-2-trifluoromethylchromone (**2**).

| Mode | Experimental | | Calculated[b] | | Assignment[c] |
|---|---|---|---|---|---|
| | IR[a] | Raman | Frequency | Intensity | |
| $\nu_1$ | 3103(vw) | – | 3224 | 4 | $\nu_{as}$ $CH_2$ |
| $\nu_2$ | 3075(vw) | 3075(38) | 3199 | 5 | ν(C1—H); ν(C2—H); ν(C3—H); ν(C9—H) |
| $\nu_3$ | – | – | 3195 | <1 | ν(C3—H); ν(C9—H); ν(C1—H) |
| $\nu_4$ | 3051(vw) | 3054(10) | 3183 | 6 | ν(C3—H); ν(C9—H) |
| $\nu_5$ | 3022(vw) | 3023(8) | 3170 | 3 | ν(C1—H); ν(C2—H) |
| $\nu_6$ | 3005(vw) | 3007(14) | 3148 | 2 | $\nu_s$ $CH_2$ |
| $\nu_7$ | 1660(vs) | 1661(100) | 1716 | 278 | ν(C=O) |
| $\nu_8$ | 1640[sh](m) | 1639(84) | 1663 | 103 | ν(C6—C7); ν(C4—C8) |
| $\nu_9$ | 1611(w) | 1611(13) | 1647 | 28 | ν(C1—C2); ν(C7—C8) |
| $\nu_{10}$ | 1579(vw) | 1582(16) | 1614 | 20 | ν(C1—C2); ν(C4—C8) |
| $\nu_{11}$ | – | – | 1505 | 7 | δ(C2—H); δ(C3—H); ν(C9—H) |
| $\nu_{12}$ | 1470(s) | 1468(9) | 1495 | 125 | δ(C11—H); δ(C1—H); δ(C2—H) |
| $\nu_{13}$ | 1434(w) | 1434(7) | 1488 | 15 | δ $CH_2$ |
| $\nu_{14}$ | 1409(s) | 1406(11) | 1407 | 91 | δ(C2—H); ν(C5—C6); ν(C7—O1); δ(C11—H) |
| $\nu_{15}$ | 1365(vw) | 1338(24) | 1363 | 1 | ν(C2—C3); ν(C4—C8); ν(C9—C1) |
| $\nu_{16}$ | 1301(s) | – | 1316 | 130 | δ(C1—H); δ(C2—H); δ(C3—H); δ(C9—H) |
| $\nu_{17}$ | 1250(s) | 1249(29) | 1262 | 45 | Wagg. $CH_2$ |
| $\nu_{18}$ | – | – | 1250 | 240 | δ(C3—H); δ(C9—H); ν(C8—O1) |
| $\nu_{19}$ | 1229(vs) | 1232(29) | 1245 | 78 | δ(C2—H); δ(C1—H) |
| $\nu_{20}$ | 1216(vs) | 1216(18) | 1233 | 47 | δ(C6—C11—H); δ(C4—C3—H); δ(C1—C2—H) |
| $\nu_{21}$ | 1192(vs) | 1180(13) | 1190 | 101 | δ(C9—C1—H); δ(C3—C2—H); ν(C6—C11); ν(C7—O1) |
| $\nu_{22}$ | 1177(s) | 1154(8) | 1180 | 156 | $\nu_{as}(CF_3)$ |
| $\nu_{23}$ | – | 1145(5) | 1171 | 16 | δ(C1—H); δ(C2—H); δ(C3—H); δ(C9—H) |
| $\nu_{24}$ | 1147(vs) | 1128(6) | 1139 | 192 | δ(C2—C3—H); δ(C1—C2—H); δ(C9—C1—H) |
| $\nu_{25}$ | 1128(vs) | 1112[sh](3) | 1129 | 230 | $\nu_{as}(CF_3)$ |
| $\nu_{26}$ | 1102(m) | 1105(6) | 1118 | 40 | Twst. $CH_2$; δ(C1—C2—H); ν(C7—C10) |
| $\nu_{27}$ | 1027(w) | 1029(18) | 1048 | 6 | δ(C4—C3—H); δ(C8—C9—H); ν(C1—C2) |
| $\nu_{28}$ | – | 1008(2) | 1011 | <1 | γ(C2—H); γ(C3—H); γ(C1—H) |
| $\nu_{29}$ | 987(m) | 985(14) | 991 | 12 | $\nu_s(CF_3)$, ν(C5—C6); δ(C6—C7—O); ν(C3—C4) |
| $\nu_{30}$ | 965(w) | 970(5) | 988 | 1 | γ(C3—H); γ(C9—H); γ(C1—H) |
| $\nu_{31}$ | 928(s) | 927(15) | 938 | 48 | γ(C11—H); δ(C5—C6—C11); δ(C2—C1—C9) |
| $\nu_{32}$ | – | – | 887 | <1 | γ(C2—C3—C4); γ(C8—C9—C1) |
| $\nu_{33}$ | – | 849(6) | 860 | 1 | δ(C1—C2—C3); γ(C6—C11—H) |
| $\nu_{34}$ | – | 817(11) | 819 | 3 | γ(C6—C11—H); γ(C8—C9—C1); γ(C4—C5—C6) |
| $\nu_{35}$ | – | 803(13) | 808 | 5 | $\nu_{as}(CF_3)$; γ(C5—C11—H); γ(C1—C9—C8) |
| $\nu_{36}$ | 767(s) | 771(5) | 779 | 75 | γ(C1—H); γ(C2—H); γ(C3—H); γ(C9—H) in phase |
| $\nu_{37}$ | 727(m) | 727(53) | 728 | 13 | γ(C8—C9—C1); γ(C2—C3—C4) |
| $\nu_{38}$ | 715(m) | 716(26) | 722 | 18 | $\delta_s(CF_3)$; γ(C8—C9—C1) |
| $\nu_{39}$ | 693(w) | 694(20) | 701 | 10 | δ(C4—C8—O1); δ(C2—C1—C9) |
| $\nu_{40}$ | 681(m) | 684(6) | 690 | 3 | γ(C10a—C7—O1); γ(C3—C2—C1); γ(C4—C5—C6) |
| $\nu_{41}$ | 640(w) | 640(8) | 646 | 12 | δ(C7—C6—C11); δ(C9—C1—C2); δ(C8—C4—C3) |
| $\nu_{42}$ | 609(w) | 609(86) | 600 | 15 | ν(C11—Br); δ(C1—C9—C8); δ(C2—C3—C4) |
| $\nu_{43}$ | 589(w) | 592[sh](23) | 595 | 4 | δ(C1—C9—C8); δ(C2—C3—C4) |
| $\nu_{44}$ | 531(vw) | 531(10) | 539 | 2 | $\delta_{as}(CF_3)$ |
| $\nu_{45}$ | – | – | 535 | 1 | γ(C1—C2—C3); γ(C9—C8—C4) |
| $\nu_{46}$ | 515(vw) | 516(26) | 521 | 2 | δ(C8—C4—C5); δ(C6—C7—O1) |
| $\nu_{47}$ | – | – | 513 | 3 | $\delta_{as}(CF_3)$ |
| $\nu_{48}$ | 467(m) | 469(15) | 471 | 25 | δ(C5—C6—C7); δ(C4—C8—O1) |
| $\nu_{49}$ | 431(w) | 433(7) | 441 | 4 | γ(C2—C3—C4); γ(C8—C9—O1) |
| $\nu_{50}$ | – | – | 381 | 8 | δ(C5—C6—C11); δ(C7—C10a—F) |
| $\nu_{51}$ | – | 357(26) | 352 | 1 | γ(C5—C6—C11); γ(C7—C10a—F) |
| $\nu_{52}$ | – | 310(23) | 318 | 2 | δ(C6—C11—H) |
| $\nu_{53}$ | – | – | 303 | 1 | γ(C8—O1—C7); γ(C2—H); γ(C7—C10a—F) |
| $\nu_{54}$ | – | 295(18) | 296 | 6 | δ(C3—C4—C5); δ(C9—C8—O1); δ(C7—C10a—F) |
| $\nu_{55}$ | – | – | 289 | 2 | δ(C7—C10a—F) |
| $\nu_{56}$ | – | 235(18) | 228 | <1 | γ(C6—C7—O1) |
| $\nu_{57}$ | – | 153(28) | 165 | 3 | $\pi_{ip}(CF_3)$ |
| $\nu_{58}$ | – | 140(14) | 141 | <1 | δ(C4—C8—O1); δ(C4—C5—O2) |
| $\nu_{59}$ | – | – | 107 | 2 | γ(C6—C11—Br) |
| $\nu_{60}$ | – | – | 70 | <1 | γ(C7—C10a—F2a) |
| $\nu_{61}$ | – | – | 52 | <1 | γ(C5—C6—C11); τ(C7—C6—C11—Br) |
| $\nu_{62}$ | – | – | 33 | 1 | τ(C5—C6—C11—H) |
| $\nu_{63}$ | – | – | 13 | <1 | τ(O1—C7—C10a—F) |

[a] vs, very strong; s, strong; m, medium; w, weak; vw, very weak; sh, shoulder.
[b] 6-311++g(d,p) calculated IR frequencies ($cm^{-1}$) and intensities (km $mol^{-1}$) in parentheses.
[c] ν, δ, γ and τ represent stretching, in-plane deformation, out-of-plane deformation and torsion modes.

*Vibrational analysis*

The solid state IR and Raman spectra of **1** and **2** are shown in Figs. 6 and 7, respectively. A tentative assignment of the observed fundamental transitions to vibration modes was assisted by the corresponding theoretical calculations. The results are presented in Tables 2 and 3, respectively. Only the modes of the most relevant characteristic functional groups of the molecules will be discussed.

*3-Methyl-2-trifluoromethylchromone (**1**)*

The weak IR absorption bands observed at 3054 and 3030 $cm^{-1}$ (calculated at 3163 and 3049 $cm^{-1}$) and the Raman dispersion bands at 3005 and 2940 $cm^{-1}$ were respectively assigned to the asymmetric and symmetric stretching mode of the methyl group. The calculated asymmetric stretching at 3095 $cm^{-1}$ could not be detected in the IR spectrum, but it appears as a medium intense band at 2981 $cm^{-1}$ in the Raman spectrum. This —$CH_3$ also shows a strong IR absorption band at 1472 $cm^{-1}$ and a weak Raman dispersion band at 1470 $cm^{-1}$ attributed to one of the asymmetric deformations (calculated at 1473 $cm^{-1}$). The Raman bands observed at 1470 and 1414 $cm^{-1}$ (calc. 1473 and 1427 $cm^{-1}$) are assigned to the asymmetric and symmetric deformations of the methyl group, respectively.

The characteristic C=O stretching mode is assigned to the very strong bands observed at 1651 (IR) and 1648 $cm^{-1}$ (Raman) that is theoretically predicted as an intense bands at 1707 $cm^{-1}$ and taking into account the assignment in 6-amino-2-trifluoromethylchromone [35]. Two IR bands at 1614 (Raman: 1615 $cm^{-1}$) and 1580 $cm^{-1}$ (calc. 1674 and 1649 $cm^{-1}$) were assigned to the stretching mode of the C=C bond (C6—C7) in the heterocyclic ring and in the phenyl ring, respectively (see Table 2).

The trifluoromethyl group shows very strong IR bands at 1134 and 1107 $cm^{-1}$ (calc. 1160, 1121 and 1047 $cm^{-1}$) attributed to the $\nu_s$, $\nu_{as}$ and $\nu_{as}$ stretching modes, respectively. These vibrations appear at 1149, 1109 and 1029 $cm^{-1}$ in the Raman spectrum. Moreover, the IR absorptions at 725 $cm^{-1}$ (Ra. 725 $cm^{-1}$) can be assigned to the symmetric deformation ($\delta_s$) while the asymmetric deformations ($\delta_{as}$) do not show activity in the IR spectrum and only one Raman band is observed at 532 $cm^{-1}$ (calc. 530 $cm^{-1}$) which is attributed to the asymmetric deformation of the —$CF_3$ group.

*3-Bromomethyl-2-trifluoromethylchromone (**2**)*

The weak IR bands at 3103 and 3005 $cm^{-1}$ (calc. 3224 and 3148 $cm^{-1}$) are respectively assigned to the asymmetric and symmetric stretching mode of the —$CH_2$ group. In the Raman spectrum it is observed only a weak band at 3007 $cm^{-1}$ which is assigned to the —$CH_2$ symmetric stretching. The $CH_2$ bending mode appears as a medium intensity IR band at 1434 $cm^{-1}$ and 1250 $cm^{-1}$ (Raman: 1434 and 1249 $cm^{-1}$). The strong IR absorption at 1660 $cm^{-1}$ (calc. 1716 $cm^{-1}$) is attributed to the stretching mode of the carbonyl group. This vibration corresponds to the strongest band in the Raman spectrum observed at 1661 $cm^{-1}$. The presence of a bromine atom on the methyl group hardly affects the band spectral location when compared with **1**.

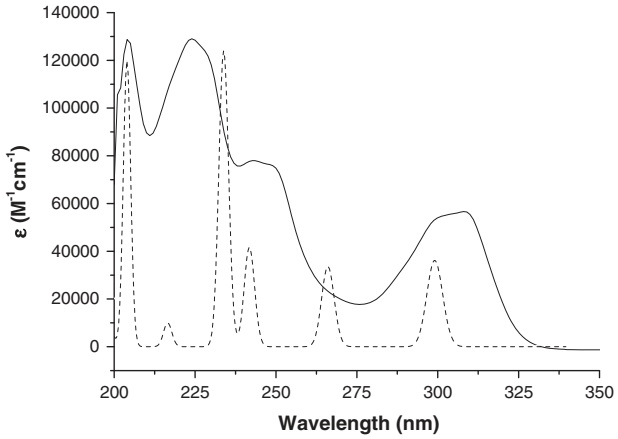


**Fig. 8.** Experimental (full trace, $7.2 \times 10^{-6}$ M in methanol) and calculated electronic spectra (B3LYP/6-311++G(d,p), dashed trace) of 3-methyl-2-trifluoromethylchromone (**1**).

The very strong IR absorptions observed at 1177, 1128 and 987 $cm^{-1}$ (Raman: 1154, 1112 (sh) and 985 $cm^{-1}$) are assigned to $CF_3$ stretching modes ($\nu_s$, $\nu_{as}$ and $\nu_{as}$, respectively) and the very weak bands located at 715 and 531 $cm^{-1}$ (Raman: 716 and 531 $cm^{-1}$) are attributed to $\delta_s$ and one of the $\delta_{as}$ $CF_3$ deformation modes. The predicted values are 722, 539 and 513 $cm^{-1}$ (see Table 3).

*Electronic spectra*

The observed electronic spectra of methanol solutions of **1** ($7.2 \times 10^{-6}$ M) and **2** ($5.9 \times 10^{-6}$ M) are respectively shown in Figs. 8 and 9 where they are compared with the corresponding theoretical spectra obtained from computed electronic transitions (see below). The observed absorption maxima for both compounds are shown in Tables 4 and 5, together with the corresponding calculated values and a tentative assignment of electronic transitions. For simplicity, only the dominant transitions (chosen in accordance with their oscillator strength) are used to assign the observed bands. Based on these results it can be concluded that the

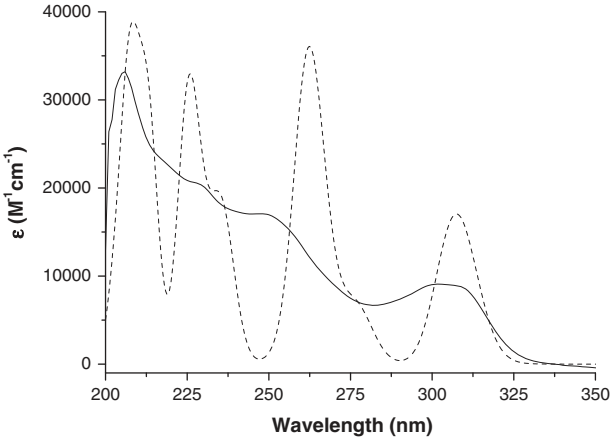


**Fig. 9.** Experimental (full trace, $5.9 \times 10^{-6}$ M in methanol) and calculated electronic spectra (B3LYP/6-311++G(d,p), dashed trace) of 3-bromomethyl-2-trifluoromethylchromone (**2**).

**Table 4**
Observed electronic spectrum of 3-methyl-2-trifluoromethylchromone (**1**) in methanol solution along with calculated electronic transitions relevant for the assignments.

| Experimental[a] | Calculated[b] (B3LYP/6-311++G(d,p)) | Assignment |
|---|---|---|
| 204 | 204 (0.354) | HOMO−2 → LUMO+1 (52%)<br>HOMO → LUMO+2 (35%)<br>HOMO−3 → LUMO+2 (13%) |
| | 217 (0.030) | HOMO → LUMO+1 (44%)<br>HOMO−2 → LUMO+1 (33%)<br>HOMO−3 → LUMO+1 (19%) |
| 224 | 234 (0.368) | HOMO−3 → LUMO (47%)<br>HOMO → LUMO+1 (40%) |
| | 242 (0.124) | HOMO−3 → LUMO (44%)<br>HOMO → LUMO+1 (43%) |
| 243[c] | 266 (0.100) | HOMO−2 → LUMO (84%)<br>HOMO → LUMO+1 (14%) |
| 308 | 299 (0.107) | HOMO → LUMO (91%) |

[a] Absorption maxima spectral positions are given in nm.
[b] Oscillator strengths of calculated transitions, shown in parenthesis, are in atomic units.
[c] Shoulder.

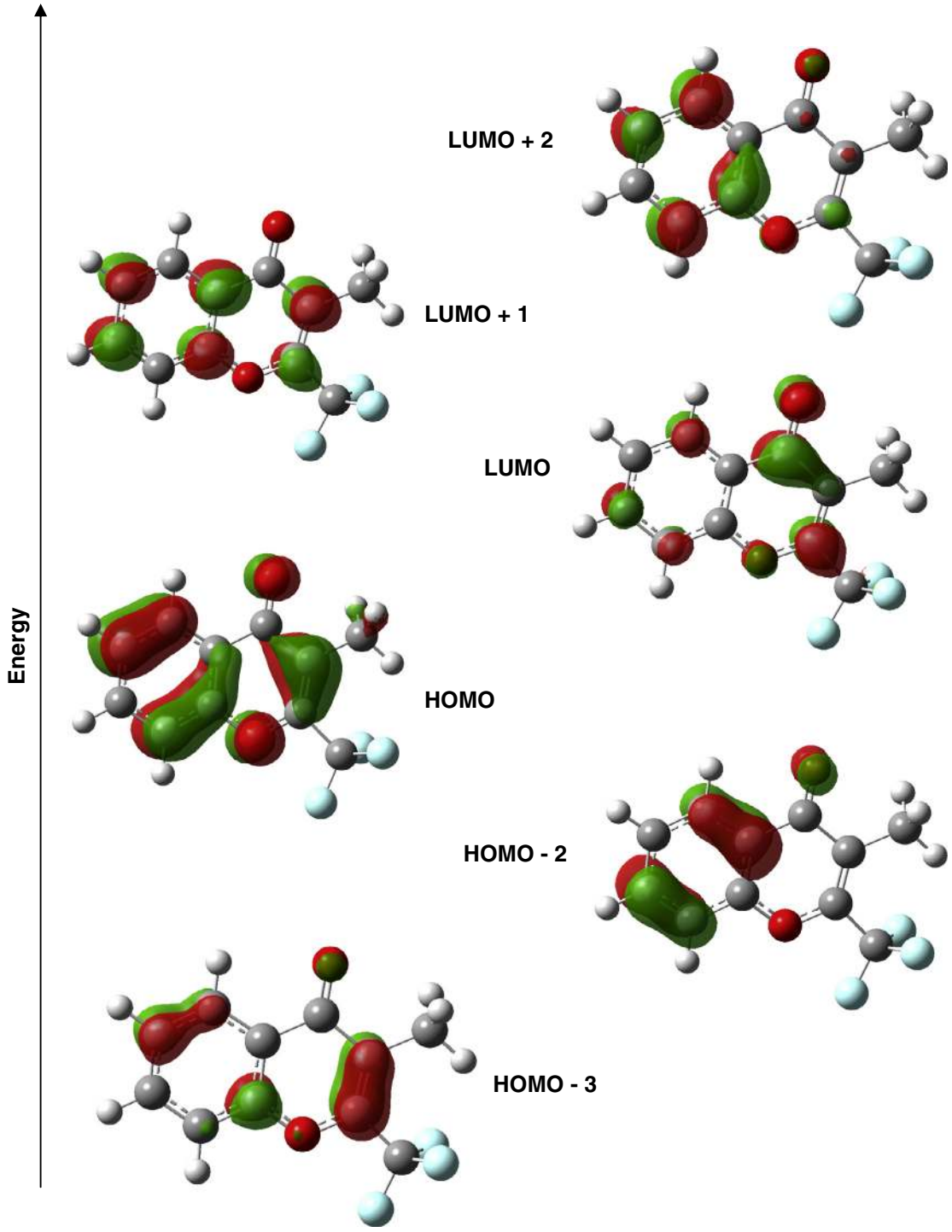


**Fig. 10.** Molecular orbitals involved in the electronic transitions of 3-methyl-2-trifluoromethylchromone (**1**). The energy scale is only qualitative and does not represent the actual energy of the molecular orbitals.

calculated transitions show a good correlation with experimental electronic spectra.

*Molecular orbitals of **1***

Fig. 10 shows the MO's (HOMO: Highest Occupied MO; LUMO: Lowest Unoccupied MO) mainly involved in the electronic transitions considered to assign the experimental bands. The observed band at 204 nm (calculated: 204 nm, see Table 4), is attributed to a one-electron transitions from HOMO−2 to LUMO+1, with minor contributions of HOMO → LUMO+2 and HOMO−3 → LUMO+2 excitations.

The absorption at 224 nm is mainly due to the contribution of one-electron HOMO to LUMO+1, HOMO to LUMO+2 and HOMO−3 to LUMO with minor contributions of other transitions. The calculated wavelengths are 217, 234 and 242 nm, respectively. The shoulder at 243 nm originates basically from HOMO−2 → LUMO one-electron excitation, which is assigned to the calculated absorption at 266 nm. Finally, the observed band at 308 nm (calc.

**Table 5**
Observed electronic spectrum of 3-bromomethyl-2-trifluoromethylchromone (**2**) along with calculated electronic transitions relevant for the assignments.

| Experimental[a] | Calculated[b] (B3LYP/6-311++G(d,p)) | Assignment |
|---|---|---|
| 202[c] | 203 (0.056) | HOMO → LUMO+3 (43%)<br>HOMO → LUMO+2 (24%)<br>HOMO−5 → LUMO+1 (22%) |
| 206 | 208 (0.222) | HOMO−2 → LUMO+3 (73%)<br>HOMO → LUMO+2 (16%)<br>HOMO → LUMO+3 (11%) |
| | 213 (0.192) | HOMO−5 → LUMO+1 (61%)<br>HOMO−2 → LUMO+2 (17%)<br>HOMO → LUMO+3 (15%) |
| | 225 (0.202) | HOMO−2 → LUMO+1 (41%)<br>HOMO−5 → LUMO (32%)<br>HOMO−5 → LUMO+1(11%)<br>HOMO−3 → LUMO+1 (11%) |
| 228[c] | 235 (0.071) | HOMO−3 → LUMO+1 (31%)<br>HOMO−4 → LUMO+1 (29%)<br>HOMO−2 → LUMO+1 (19%)<br>HOMO−5 → LUMO (11%) |
| 247[c] | 262 (0.214) | HOMO → LUMO+1 (60%)<br>HOMO−3 → LUMO (22%) |
| 302 | 308 (0.119) | HOMO → LUMO (98%) |

[a] Absorption maxima spectral positions are given in nm.
[b] Oscillator strengths of calculated transitions, shown in parenthesis, are in atomic units.
[c] Shoulder.

299 nm) is attributed to a dominant one-electron excitation from the HOMO to the LUMO.

As can be deduced from Fig. 10, the HOMO−3 MO presents a π bonding character of some carbon atoms on the aromatic ring and of the heterocyclic double bond, besides the non-bonding contributions of the carbonilic oxygen atom. The HOMO−2 is mainly localized on the phenyl ring and shows a π-bonding character and non-bonding contribution of the oxygen of the carbonyl group. Moreover, the HOMO displays a π-bonding character mostly involving the carbon atoms of both rings and a non-bonding nature of both oxygen atoms. Furthermore, the LUMO shows some π anti-bonding contributions of the carbon atoms on the benzene ring, a non-bonding character of the oxygen atoms and some carbon atoms in the heterocyclic ring.

The LUMO+1 exhibits an extended π anti-bonding character throughout both rings, whereas the LUMO+2 presents a π anti-bonding contribution in most of the carbon atoms and non-bonding character in both oxygen atoms. According to the previous analysis, it can be inferred that the experimental absorptions at 204, 224 and 308 nm correspond to transitions that involve both fused rings. The band at 243 nm is mainly dominated by transitions from the aromatic to the heterocyclic ring (see Table 4).

*Molecular orbitals of **2***

The MO's mainly involved in the electronic transitions used to assign the bands of the experimental spectrum are depicted in Fig. 11. The shoulder at 202 nm is attributed to one-electron transitions from HOMO to LUMO+3 and to minor contributions of HOMO to LUMO+2 and HOMO−5 to LUMO+1, which is assigned to the transition calculated to occur at 203 nm (see Table 5).

The intense band at 206 nm arises mainly of one-electron excitation from HOMO−2 to LUMO+3 (calc. 208 nm) and HOMO−5 to LUMO+1 (calc. 213 nm) along with other small contributions of one-electron transitions. The shoulder at 228 nm originates basically from HOMO−2 → LUMO+1 and HOMO−5 → LUMO (calc. 225) and from HOMO−3 → LUMO+1 and HOMO−4 → LUMO+1 (calc. 235 nm) one-electron excitations. The observed shoulder at 247 nm (calc. 262 nm) is attributed to a nearly dominant one-electron excitation from HOMO → LUMO+1 with minor contribution of HOMO−3 → LUMO. The absorption at 302 nm is dominated by a one-electron excitation from the HOMO to the LUMO and assigned to the transition calculated at 308 nm.

As can be observed in Fig. 11, the HOMO, involves the π-bonding orbitals of the aromatic ring and the non-bonding character of both oxygen and of some carbon atoms. HOMO−2 is basically localized on the π-bonding orbitals of the benzenic ring and on the non-bonding orbital of the carbonilic oxygen. HOMO−3, HOMO−4 and HOMO−5 MO's principally involve the non-bonding character of the bromine and both oxygen atoms, whereas HOMO−5 presents besides the contribution of the π-bonding orbital of the double bond in the heterocyclic ring.

The LUMO exhibits π anti-bonding character of the carbon atoms on the aromatic ring and non-bonding character of some carbon and both oxygen atoms. The LUMO+1 presents an extended π anti-bonding character throughout both rings and non-bonding contribution of the bromine atom. LUMO+2 is mainly localized on the aromatic ring and shows π anti-bonding character, while LUMO+3 exhibits a *d* character on the bromine atom and π anti-bonding contribution of both rings. From the preliminary analysis it can be argued that the shoulder at 202 nm corresponds to transitions from the π-bonding orbitals of both rings and from the non-bonding orbitals of both oxygen atoms to the aromatic moiety of the molecule and to the bromine atom. The bands at 206, 228 and 247 nm are due to transitions that involve both fused rings, with minor contribution of transitions in the aromatic ring and with participation of the non-bonding and *d* orbitals of the bromine atom. The band at 302 nm is mainly dominated by a transition from both rings to the heterocycle (see Table 5).

*NMR spectra*

After full geometry optimization with the GAUSSIAN 03 program package (see 'Computational methods' in 'Experimental section') the $^{1}H$, and $^{13}C$ chemical shifts ($\delta$) were calculated with the GIAO method [30]. Table 6 shows the experimental and calculated chemical shifts using the B3LYP method and the triple-ζ basis set 6-311+g(2d,p) for both **1** and **2** compounds. All data sets showed a linear relationship with *R*-square values for each compound above 0.995.

The following correlations $\delta_{calc} = a\ \delta_{exp} + b$ given in Fig. S4(a–d) (Supporting Information) were obtained. Fig. **a**: ($R^2 = 0.998$; $a = 1.069$; $b = 0.271$); Fig. **b**: ($R^2 = 0.995$; $a = 1.021$; $b = 3.783$); Fig. **c**: ($R^2 = 0.995$; $a = 1.016$; $b = 0.104$), and Fig. **d**: ($R^2 = 0.992$; $a = 0.908$; $b = 18.75$). Comparing the experimental and theoretical data of protons, a good agreement is observed with $\Delta = \delta_{exp} - \delta_{calc}$ deviation ranging from −0.1 to +0.5 and from +0.2 to +0.4 ppm for **1** and **2**, respectively.

The $\Delta$-values found for the carbon atoms differ in up to 17.2 ppm. The greatest discrepancy was found for **2** in the prediction of the —$CH_2$Br chemical shift, with values of $\Delta = 17.2$ ppm (see Table 6). This fact suggests that the presence of the heavy atom produces an appreciable diamagnetic shielding on the carbon atom due to its large number of electrons. The calculations overestimate the inductive effect of the bromine atom that actually should deshield the alpha carbon [36]. Moreover, a strong divergence was found in the chemical shift of halogenated compounds inclusive with those calculated at a relativistic approach with BP86 [37].

Furthermore, calculations also fail in describe correctly the experimental data of carbon atoms in the trifluoromethyl group with values of $\Delta = -12.2$ and −12.0 ppm for **1** and **2**, respectively (see Table 6). The isotropic shielding of the fluorine atoms is underestimated by theoretical calculations as observed in some

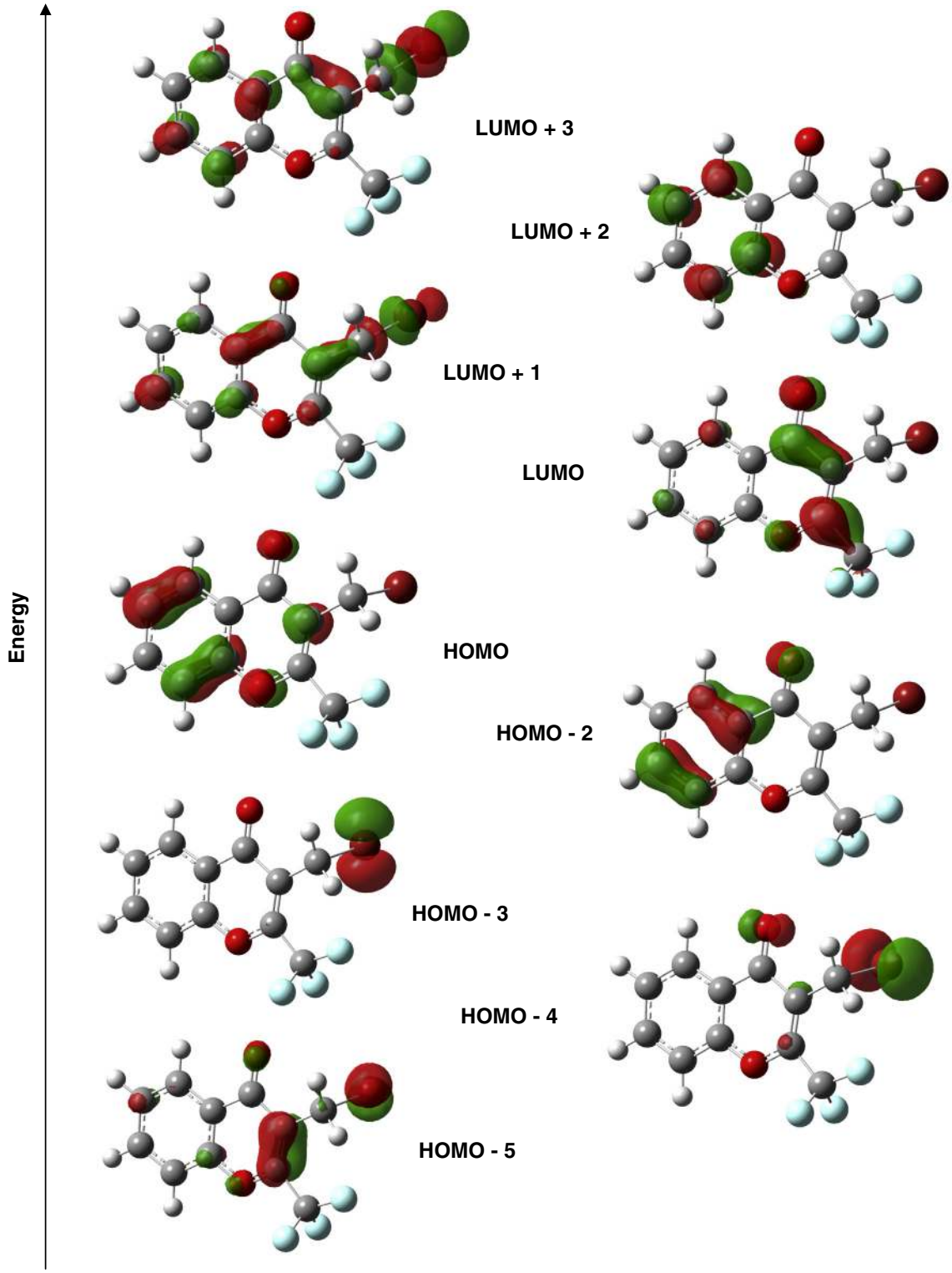


**Fig. 11.** Molecular orbitals involved in the electronic transitions of 3-bromomethyl-2-trifluoromethylchromone (**2**). The energy scale is only qualitative and does not represent the actual energy of the molecular orbitals.

trifluoromethyl tetraisoquinolines [38] and trifluoromethyl chromones [35].

## Conclusions

As noted by quantum chemical calculations and X-ray crystal structure results, the title compounds exhibit both planar conformations due to an extensive π-bonding conjugation, which extends almost along the whole molecule. The comparison between theoretical and experimental structural parameters is also in good agreement, showing that no drastic changes occurs going from solid to gas phase. Taking into account both crystal structures, the distinction occurs in the bromo-substituted chromone since the bulky bromine atom prevents the efficiency of

**Table 6**
Comparison between experimental and B3LYP calculated NMR chemical shifts (in ppm) for **1** and **2**.[a]

| | 1 | | | | 2 | | |
|---|---|---|---|---|---|---|---|
| | Exp. | 6-311+g(2d,p) | | | Exp. | 6-311+g(2d,p) | |
| $CH_3$ | 2.23 | 2.13 | (0.1) | $C\underline{H}_2$ | 4.56 | 4.77 | (−0.21) |
| 5-H | 8.19 | 8.65 | (−0.5) | 5-H | 8.23 | 8.63 | (−0.4) |
| 6-H | 7.44 | 7.69 | (−0.3) | 6-H | 7.52 | 7.71 | (−0.19) |
| 7-H | 7.72 | 7.87 | (−0.1) | 7-H | 7.79 | 7.94 | (−0.15) |
| 8-H | 7.51 | 7.69 | (−0.2) | 8-H | 7.54 | 7.70 | (−0.16) |
| 2-C | 148.2 | 156.0 | (−7.8) | 2-C | 149.9 | 156.9 | (−7.0) |
| 3-C | 120.9 | 128.9 | (−8.0) | 3-C | 121.4 | 131.8 | (−10.4) |
| 4-C | 177.9 | 181.8 | (−3.9) | 4-C | 175.4 | 179.8 | (−4.4) |
| 5-C | 126.1 | 132.4 | (−6.3) | 5-C | 122.7 | 132.8 | (−10.1) |
| 6-C | 125.9 | 129.9 | (−4.0) | 6-C | 126.4 | 131.0 | (−4.6) |
| 7-C | 134.6 | 138.4 | (−3.8) | 7-C | 135.4 | 139.6 | (−4.2) |
| 8-C | 118.2 | 122.2 | (−4.0) | 8-C | 118.4 | 121.9 | (−3.5) |
| 4a-C | 122.4 | 128.9 | (−6.5) | 4a-C | 122.7 | 128.1 | (−5.4) |
| 8a-C | 155.1 | 161.9 | (−6.8) | 8a-C | 154.9 | 161.5 | (−6.6) |
| $CH_3$ | 8.7 | 12.4 | (−3.7) | $\underline{C}H_2Br$ | 18.8 | 36.0 | (−17.2) |
| $CF_3$ | 120.0 | 132.2 | (−12.2) | $CF_3$ | 119.4 | 131.4 | (−12.0) |

[a] $\Delta = \delta_{exp} - \delta_{calc}$ values in parentheses. The standard numbering scheme of the benzopyrane skeleton was adopted for atoms labeling.

the packing and allows the observed rotational disorder around the C—$CF_3$ bond. This result was supported by theoretical calculations, which predict a very low energy barrier for the O1C7C10F3 dihedral angle and the possibility of multiple rotamers. The GIAO approach is appropriate for predicting the $^1H$ and $^{13}C$ chemical shifts in both compounds, but it underestimates the isotropic shielding of the strong electron withdrawing fluorine and the bulky bromine atoms. In the last case, the disagreement between $^{13}C$ calculated and experimental chemical shifts is attributed to the heavy atom effect. In addition, the calculated vibrational (IR and Raman) and electronic spectra are in good accordance with the experimental ones, supporting the assignment of the observed bands.

## Acknowledgements

The authors thank Universidad Nacional de La Plata (UNLP), CONICET, DAAD-Germany, and Departamento de Ciencias Básicas de la Universidad Nacional de Luján for financial support. S.E.U and J.L.J specially thanks Deutscher Akademischer Austauschdienst Germany (DAAD) for an equipment grant and financial support. CDAL thanks SENESCYT- Ecuador for the fellowship and financial support. The crystallographic work was supported by CONICET (PIP 1529), and by ANPCyT (PME06 2804 and PICT06 2315) of Argentina. S.E.U, G.A.E and O.E.P are research fellows of CONICET.

## Appendix A. Supplementary material

Supplementary data associated with this article can be found, in the online version, at http://dx.doi.org/10.1016/j.saa.2014.10.022.

## References

[1] L.D. Quin, J. Tyrell, Fundamentals of Heterocyclic Chemistry: Importance in Nature and in the Synthesis of Pharmaceuticals, Wiley, 2010.
[2] T. Eicher, S. Hauptmann, A. Speicher, The Chemistry of Heterocycles, Wiley, 2003.
[3] J.A. Joule, K. Mills, Heterocyclic Chemistry, John Wiley & Sons, 2010.
[4] G.P. Ellis, The Chemistry of Heterocyclic Compounds, Chromenes, Chromanones, and Chromones, Wiley, 2009.
[5] E. Grotewold, The Science of Flavonoids, Springer, 2007.
[6] B.M. Fraga, A.G. González, O. Pino, Distribución de las cromonas en la naturaleza∗ Cromonas del Cneorum tricoccum L, Anal. Quim. 71 (1975) 347–369.
[7] M.T. Giardi, G. Rea, B. Berra, Bio-Farms for Nutraceuticals: Functional Food and Safety Control By Biosensors, Landes Bioscience, 2010.
[8] G.G. Chabot, Y.S. Touil, M.H. Pham, D. Dauzonne, Flavonoids in cancer prevention and therapy: chemistry, pharmacology, mechanisms of action, and perspectives for cancer drug discovery, in: M. Alaoui-Jamali (Ed.), Alternative and Complementary Therapies for Cancer, Springer, US, 2010, pp. 583–612.
[9] E.S.C. Wu, J.T. Loch, B.H. Toder, A.R. Borrelli, D. Gawlak, L.A. Radov, N.P. Gensmantel, Flavones. 3. Synthesis, biological activities, and conformational analysis of isoflavone derivatives and related compounds, J. Med. Chem. 35 (1992) 3519–3525.
[10] X. Wu, S. Yin, J. Zhong, W. Ding, J. Wan, Z. Xie, Mushroom tyrosinase inhibitors from Aloe barbadensis Miller, Fitoterapia 83 (2012) 1706–1711.
[11] B. China Raju, R. Nageswara Rao, P. Suman, P. Yogeeswari, D. Sriram, T.B. Shaik, S.V. Kalivendi, Synthesis, structure–activity relationship of novel substituted 4H-chromen-1,2,3,4-tetrahydropyrimidine-5-carboxylates as potential anti-mycobacterial and anticancer agents, Bioorg. Med. Chem. Lett. 21 (2011) 2855–2859.
[12] J. Ungwitayatorn, C. Wiwat, W. Samee, P. Nunthanavanit, N. Phosrithong, Synthesis, in vitro evaluation, and docking studies of novel chromone derivatives as HIV-1 protease inhibitor, J. Mol. Struct. 1001 (2011) 152–161.
[13] Y. Chen, H.-R. Liu, H.-S. Liu, M. Cheng, P. Xia, K. Qian, P.-C. Wu, C.-Y. Lai, Y. Xia, Z.-Y. Yang, S.L. Morris-Natschke, K.-H. Lee, Antitumor agents 292. Design, synthesis and pharmacological study of S- and O-substituted 7-mercapto- or hydroxy-coumarins and chromones as potent cytotoxic agents, Eur. J. Med. Chem. 49 (2012) 74–85.
[14] A.Y. Shaw, C.-Y. Chang, H.-H. Liau, P.-J. Lu, H.-L. Chen, C.-N. Yang, H.-Y. Li, Synthesis of 2-styrylchromones as a novel class of antiproliferative agents targeting carcinoma cells, Eur. J. Med. Chem. 44 (2009) 2552–2562.
[15] D.F. Liu, C.C. Cheng, A facile and practical preparation of 5,7-dihydroxy-3-(4-nitrophenyl)-4H-1-benzopyran-4-one, J. Heterocyclic Chem. 28 (1991) 1641–1642.
[16] P.K. Zubaidha, A.M. Hashmi, R.S. Bhosale, FeCl3 catalyzed dehydrative cyclisation of 1,3-(diaryl diketones) to flavones, Heterocycl. Commun. 11 (2005) 97–100.
[17] Q. Yang, H. Alper, Synthesis of chromones via palladium-catalyzed ligand-free cyclocarbonylation of o-iodophenols with terminal acetylenes in phosphonium salt ionic liquids, J. Org. Chem. 75 (2010) 948–950.
[18] J. Santamaría, C. Valdés, Six-membered rings with one oxygen: pyrylium ion, related systems and benzo-derivatives, in: J. Alvarez-Builla, J.J. Vaquero, J. Barluenga (Eds.), Modern Heterocyclic Chemistry, Wiley-VCH Verlag GmbH & Co. KGaA, Weinheim, Germany, 2011, pp. 1631–1682 (Chapter 18).
[19] V.Y. Sosnovskikh, B.I. Usachev, A convenient synthesis of 4(5)-(2-hydroxyaroyl)-5(4)-trifluoromethyl-1,2,3-triazoles from 2-trifluoromethylchromones and chromen-4-imines, Mendeleev Comm. 12 (2002) 75–76.
[20] V.Y. Sosnovskikh, M.A. Barabanov, The first synthesis of 8-aza-2-polyfluoroalkylchromones, J. Fluorine Chem. 120 (2003) 25–28.
[21] V.Y. Sosnovskikh, B.I. Usachev, D.V. Sevenard, G.-V. Röschenthaler, Nucleophilic trifluoromethylation of RF-containing 4-quinolones, 8-aza- and 1-thiochromones with (trifluoromethyl)trimethylsilane, J. Fluorine Chem. 126 (2005) 779–784.
[22] V.Y. Sosnovskikh, V.Y. Korotaev, A.Y. Barkov, A.A. Sokovnina, M.I. Kodess, Reaction of 2-(trifluoromethyl)chromones with pyridoxal: formation of 1-benzopyranooxepino- and 1-benzopyranopyranopyridines, J. Fluorine Chem. 141 (2012) 58–63.
[23] I.C.H. Castañeda, S.E. Ulic, C.O.D. Védova, N. Metzler-Nolte, J.L. Jios, One-pot synthesis of 2-trifluoromethylchromones, Tetrahedron Lett. 52 (2011) 1436–1440.
[24] CrysAlisPro, Oxford Diffraction Ltd., 2009.
[25] G.M. Sheldrick, SHELXS-97. Program for Crystal Structure Resolution, University of Göttingen, Göttingen, Germany, 1997.
[26] G.M. Sheldrick, SHELXL-97. Program for Crystal Structures Analysis, Univ. of Göttingen, Göttingen, Germany, 1997.
[27] M.J. Frisch, G.W. Trucks, H.B. Schlegel, G.E. Scuseria, M.A. Robb, J.R. Cheeseman, J.A. Montgomery Jr., T. Vreven, K.N. Kudin, J.C. Burant, J.M. Millam, S.S. Iyengar, J. Tomasi, V. Barone, B. Mennucci, M. Cossi, G. Scalmani, N. Rega, G.A. Petersson, H. Nakatsuji, M. Hada, M. Ehara, K. Toyota, R. Fukuda, J. Hasegawa, M. Ishida, T. Nakajima, Y. Honda, O. Kitao, H. Nakai, M. Klene, X. Li, J.E. Knox, H.P. Hratchian, J.B. Cross, C. Adamo, J. Jaramillo, R. Gomperts, R.E. Stratmann, O. Yazyev, A.J. Austin, R. Cammi, C. Pomelli, J.W. Ochterski, P.Y. Ayala, K. Morokuma, G.A. Voth, P. Salvador, J.J. Dannenberg, V.G. Zakrzewski, S. Dapprich, A.D. Daniels, M.C. Strain, O. Farkas, D.K. Malick, A.D. Rabuck, K. Raghavachari, J.B. Foresman, J.V. Ortiz, Q. Cui, A.G. Baboul, S. Clifford, J. Cioslowski, B.B. Stefanov, G. Liu, A. Liashenko, P. Piskorz, I. Komaromi, R.L. Martin, D.J. Fox, T. Keith, M.A. Al-Laham, C.Y. Peng, A. Nanayakkara, M. Challacombe, P.M.W. Gill, B. Johnson, W. Chen, M.W. Wong, C. Gonzalez, J.A. Pople, Gaussian 03, Gaussian Inc, Pittsburgh PA, 2003.
[28] P. Elliott, F. Furche, K. Burke, Excited states from time-dependent density functional theory, Rev. Comp. Chem. 26 (2009) 91–166.
[29] A. Dreuw, M. Head-Gordon, Single-reference ab initio methods for the calculation of excited states of large molecules, Chem. Rev. 105 (2005) 4009–4037.
[30] R. Ditchfield, Self-consistent perturbation theory of diamagnetism, Mol. Phys. 27 (1974) 789–807.
[31] V.Y. Sosnovskikh, R.A. Irgashev, V.S. Moshkin, M.I. Kodess, Reaction of 3-(polyfluoroacyl)chromones with hydrazines: new regioselective synthesis of RF-containing pyrazoles, Russian Chem. Bull. Int. Ed. 57 (2008) 2146–2155.

[32] A. Spek, PLATON, an integrated tool for the analysis of the results of a single crystal structure determination, Acta Crystallogr. Sect. A 46 (1990) c34.
[33] A.L. Spek, PLATON, A Multipurpose Crystallographic Tool, Utrecht University, Utrecht, The Netherlands, 1998.
[34] C.P. Slichter, Principles of Magnetic Resonance, Springer-Verlag, Heidelberg, 1990.
[35] L.P. Avendaño Jiménez, G. Echeverría, O.E. Piro, S.E. Ulic, J.L. Jios, Vibrational, electronic and structural properties of 6-nitro- and 6-amino-2-trifluoromethylchromone: an experimental and theoretical study, J. Phys. Chem. A. 117 (2013) 2169–2180.
[36] F.D.P. Morisso, H. Stassen, P.R. Livotto, V.E.U. Costa, 1H and 13C chemical shift calculations for 12-oxa-pentacyclo[6.2.1.16,9.02,7.02,10]dodeca-4-eno systems using GIAO method at different levels of theory, J. Mol. Struct. 738 (2005) 281–290.
[37] A.C. Neto, L.C. Ducati, R. Rittner, C.F. Tormena, R.H. Contreras, G. Frenking, Heavy halogen atom effect on 13C NMR chemical shifts in monohalo derivatives of cyclohexane and pyran. Experimental and theoretical study, J. Chem. Theory Comput. 5 (2009) 2222–2228.
[38] I. Cakmak, GIAO calculations of chemical shifts in enantiometrically pure 1-trifluoromethyl tetrahydroisoquinoline alkaloids, J. Mol. Struct. (THEOCHEM) 716 (2005) 143–148.